A Novel Control Strategy to Active Power Filter with Load Voltage Support Considering Current Harmonic Compensation

Saeedeh Torabi Jafrodi [1], Mojgan Ghanbari [2], Mehrdad Mahmoudian [3], Arsalan Najafi [4],*, Eduardo M. G. Rodrigues [5],* and Edris Pouresmaeil [6]

[1] Sazeh Consultant Co. (Engineering & Construction), Tehran 15876, Iran; torabi_s90@yahoo.com
[2] Department of Electrical Engineering, Islamic Azad University, Saveh Branch, Saveh 39197, Iran; m.ghanbari0@yahoo.com
[3] Firouzabad Institute of Higher Education, Firouzabad 74717, Iran; m.mahmoodian@fabad-ihe.ac.ir
[4] Young Researchers and Elite Club, Sepidan Branch, Islamic Azad University, Sepidan 73611, Iran
[5] Management and Production Technologies of Northern Aveiro—ESAN, Estrada do Cercal 449, Santiago de Riba-Ul, 3720-509 Oliveira de Azeméis, Portugal
[6] Department of Electrical Engineering and Automation, Aalto University, 02150 Espoo, Finland; edris.pouresmaeil@aalto.fi
* Correspondence: arsalan.najafi@iausepidan.ac.ir (A.N.); emgrodrigues@ua.pt (E.M.G.R.)

Abstract: This paper outlines some modifications to conventional active power filters (APFs) to compensate for the non-linearity of the load current. Since the APFs inject the required non-linearity of the load harmonic current to make the current source sinusoidal, a combination of passive power filters (PPFs) and APFs in series connection are more effective rather than individual usages. The proposed control approach based on sliding mode control (SMC) with a suitable sliding surface selection being applied to the proposed hybrid APF to increase the flexibility and reduce the complexity of the controller. An outstanding tracking process based on the reference current in the rotating *dq* frame is tested and guarantees the rapid convergence exponentially. An extra control loop is provided for DC link voltage regulation to minimize the DC ripples and control the APF three-phase output voltage levels. The presented solution provides an effective and straightforward load voltage support, maintaining an excellent dynamic performance in load changing and current compensation. The experimental results represent the authenticity of the proposed hybrid APF performance through several different tests, implying a feasible control approach for active filtering systems.

Keywords: active power filter; control; harmonic compensation

1. Introduction

The usage of power quality compensators in the distribution system has been increased in recent years due to the increasing number of non-linear loads connected to the grid. This can cause power quality deterioration such as unbalancing, over-loading, over-voltage, under-voltage, voltage sag, and swell, which affect the performance of sensitive loads [1]. The utilization of active power filters (APFs) to solve and maintain the load voltage and grid non-linearity currents problems has been one of the appropriate approaches that has received much attention in recent years. These filters are connected in series or parallel to the power system to compensate the harmonics, load balancing, reactive power control, and the null wire current recompensing if used. The APFs also have the capability of being integrated as a combination of an APF and a parallel, which are studied in the flexible AC transmission system (FACTS) field. The series active filter, which is controlled by a non-sinusoidal voltage source,

has the function of compensating the grid voltage. In this case, using an integrated quality controller, even with harmonics in the load current and voltage, can assure that there is a regulated voltage with a low harmonic value [2–4].

Actually, the APFs as harmonic compensators based on a power electronics interface have been the focus of many researchers and industries due to their simple structure and non-complexity. Power electronics converters as the main part of these devices have been reviewed in prestigious literatures from different points of view [5,6]. In the general classification, the converters used include voltage source inverters (VSIs) and current source inverters (CSIs). VSIs have been introduced in multi-level and multi-phase types, while in recent years, multi-level CSIs have been designed and implemented for harmonic compensation [7]. Likewise, CSIs have undergone their laboratory and industrial evolution and performance reporting and are presented in valid different structures [8]. These converter losses can be classified into four subdivisions, including passive output filter losses (AC losses), conduction losses, switching losses of power switches, and DC-side losses. Semiconductor conductive losses due to equivalent resistance and voltage drop in the conducting state and switching losses are due to the improper operation of the switches [9,10].

In recent years, there have been many researches conducted on APF performance evaluation for load compensating. For example, the authors in [11] present the idea of using two VSI and CSI simultaneously. Since the load current and therefore the reference current comprises different harmonic components, it can play a significant role in dividing the reference current between the two converters with different separating. The differential behavior of DC capacitors and DC inductors in high-frequency and low-frequency currents is important for how the reference current is split between the CSI and the VSI. Based on the obtained mathematical equations, if the proposed low-frequency components are applied to the CSI and the high-frequency components are applied to the VSI, the proposed APF can meet the design objectives. A classic APF contains a VSI with a three-leg bridge structure and a DC link capacitor, whose topologies require a matching transformer and a large number of active switching devices, which causes many disadvantages, especially in losses. These considerations result in heavy weight and an expensive system [12]. The conceptual design of the components of this integrated active filter is presented in [13]. By determining the CSI and VSI contribution to the harmonic filter of the load current, the size of the passive elements on the DC and AC sides, as well as the switching frequency, are determined. This design is based on the resulting equivalent circuit and simple KVL principles as well as the commonly accepted criteria. The results of the analysis show how and under what conditions the size of the passive elements in the proposed structure is reduced compared to the conventional ones. However, although the theoretical foundations of the size of the passive elements in the DC and AC sides of the converters in the integrated APF structure are explained in [14], it is necessary to calculate and evaluate the impact of this reduction on the overall filter losses by mathematical analysis.

The concept of current compensation by APFs has been drawn intuitively for better understanding in Figure 1. It is assumed that a non-linear or unbalanced load is going to be fed through an AC power source. Since the AC source should not generate the pulsating current due to the safety and lifetime procedures, the sinusoidal current waveform is just allowed to be injected to the grid according to power quality standards. Therefore, the non-linearity components of the required current are supplied by the AFP [15–18]. In order to decrease the output voltage ripples using only passive filters, the switching frequency is increased, which results in incremental switching losses a reduction in the system's efficiency. Other disadvantages of these filters are their strong dependence on the resonant frequency to the equivalent impedance of the grid. Reducing the switching loss and switching noise requires the soft-switching circuit and implementing the dynamic reactive power compensation capability, which has been presented in [19]. Therefore, a quasi-DC link voltage-controlled loop in the APF control method is added. However, the proposed adaptive DC control algorithm excludes current harmonic consideration.
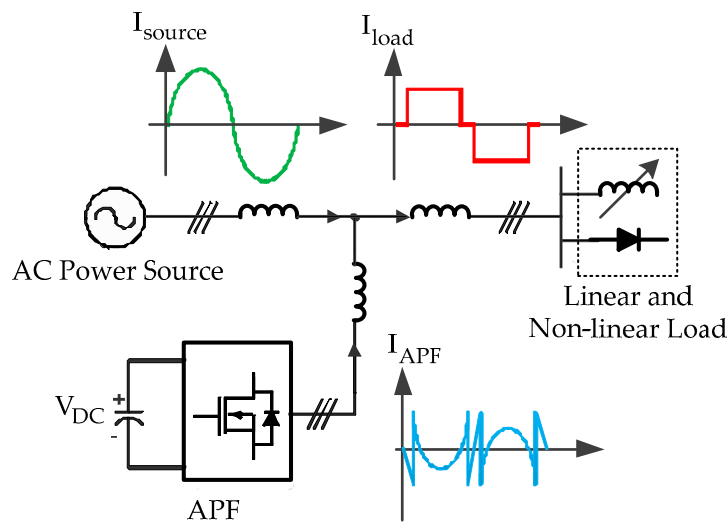
Figure 1. The active power filter (APF) current compensation concept.

In this paper, a hybrid APF with current harmonic compensation is proposed to maintain the AC power source sinusoidal. The SMC approach is utilized for load voltage support and appropriate reference signal tracking. Briefly, the contributions of this manuscript are listed below:

- An L-C passive filter is connected in series with an APF to compensate the current harmonic. It improves the system efficiency with an extra opportunity in conditions of whether the APF is participating in the compensation process or not.
- The SMC approach makes the convergence more achievable, especially in non-linear systems such as the APF injection current.
- The control approach is capable of overcoming the voltage unbalancing.
- The coding and implementation of the proposed strategy have removed the complexity of the conventional approach.
- The power-factor correction (PFC) and reactive power control are accessible.

2. Hybrid Active Power Filter Concept

Usually, most of the power electronics loads in the distribution network such as rectifiers, thyristors, etc., are non-linear and generate unsolicited harmonics. An individual inductor is the simplest structure as a filter that is not commonly used for medium and high-power converters due to problems such as voltage reductions in the DC side of the inverter, low dynamic converter efficiency, cost increment, and low power density [20–22]. The LCL filter is an attractive solution to overcome the problems mentioned, which improves the harmonic mitigation at lower switching frequency [23]. Nowadays, the most common device used to support the load voltage is a shunt capacitor, which could also improve the reactive power. However, they suffer from harmonics existing in the power grid, which makes them explode. A few later, the passive power filters (PPFs) were developed to compensate for the non-linearity components through series or parallel connections. Their advantages include simplicity in installation, but they were bulky and expensive. Therefore, the APFs have come into the industries to overcome all the drawbacks declared above. The most important issue in operating APFs is how to control and connect them to the power grid. Since in APFs, both the DC link voltage and load current harmonics must be fully controlled, consequently, several nested control loops are usually required to be designed and implemented. In addition, their switching and conduction losses are added to the total system losses, and if an appropriate switching algorithm is not selected, it may greatly reduce the overall efficiency. Various APFs have been introduced so far, with different applications depending on how they are controlled and connected to the network [24–29]. A new type of compensator that uses

both APFs and PPFs to improve performance is called hybrid APF, which has received much more attention than the conventional ones [30].

APFs are usually divided into different categories according to their operation modes, control strategy, series and parallelism connections, etc. Figure 2 shows the various topologies of APFs that have been presented so far [28]. Figure 2a shows a four-switch APF controlled by two proportional integrator (PI) controllers to provide gate pulses of power switches in each inverter legs. Another PI controller is used to adjust the DC link voltage to make the inverter output voltage regulated. This APF is categorized in a parallel classification that can supply the non-linear required load current. A nine-switch AC/AC converter with a quasi-DC link is presented in Figure 2b to compensate the non-linear load current. This APF topology is inflexible regarding controlling the power switches. A full bridge type of conventional APF with an eight-switch four-leg converter is shown in Figure 2c, in which the separated DC link voltage into two parts facilitates the zero-current component recognition.
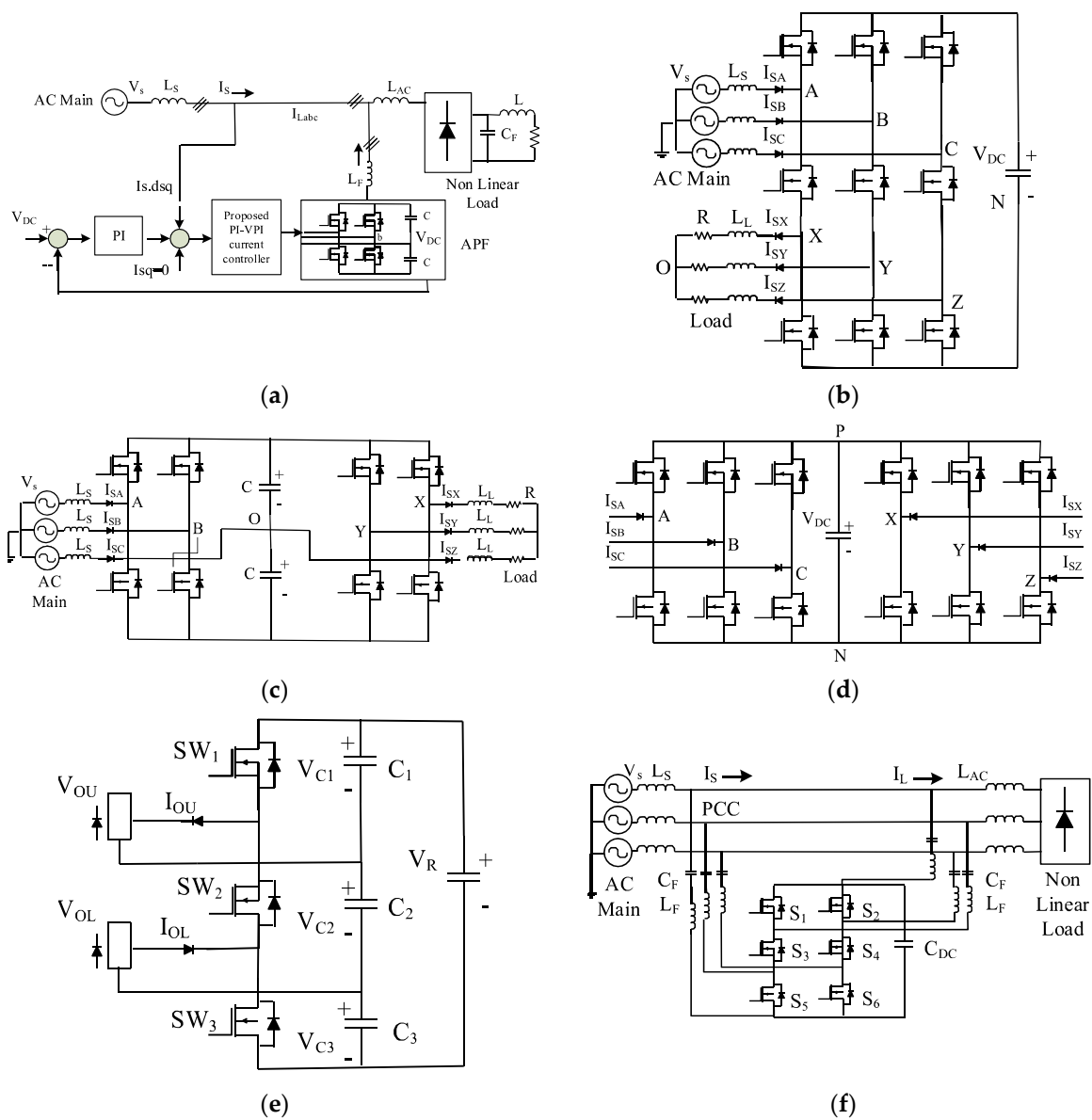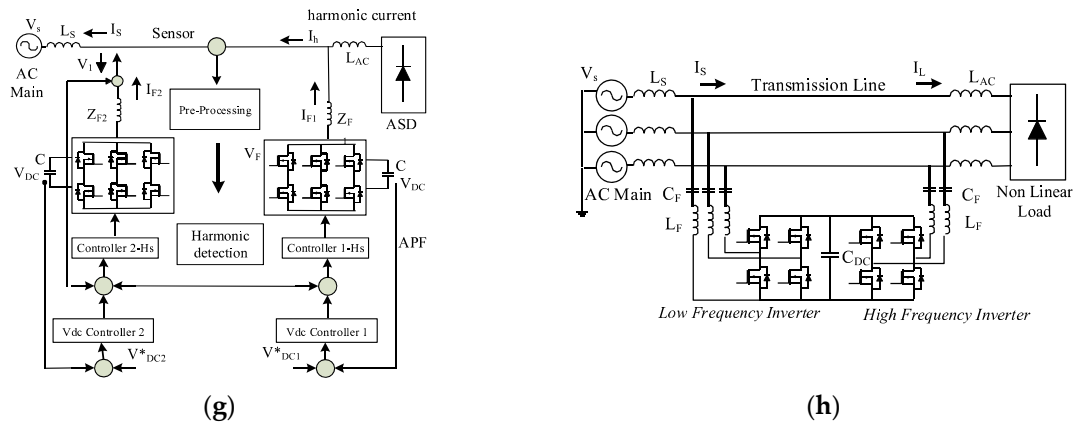

(**a**)

(**b**)

(**c**)

(**d**)

(**e**)

(**f**)

Figure 2. *Cont.*

(**g**)　　　　　　　　　　　　　(**h**)

Figure 2. The conventional APFs; (**a**) four-switch three phase shunt APF, (**b**) nine-switch AC/AC converter with a quasi-DC link, (**c**) eight-switch four-leg converter, (**d**) back-to-back two level voltage source converter (VSC), (**e**) three-switch three-capacitor multi-level inverter (MLI), (**f**) six-switch two leg inverter, (**g**) 12-switch APF with feedback harmonic detection, (**h**) eight-switch dual parallel full bridge inverter, Reproduced with permission from [28], Copyright Elsevier, 2017.

Figure 2d is dedicated a back-to-back two-level voltage source converter (VSC) to compensate for the load current harmonics. The quasi DC link voltage between the load and the AC source provides a better capacitive current injection. In Figure 2e, a three-switch three-capacitor multi-level inverter (MLI) is proposed as a parallel APF. This topology is capable of compensating for the non-linear load current, but the non-inductive properties of the APF are the drawbacks of the control method. A six-switch two-leg inverter is represented in Figure 2f with a hybrid connection between the AC source and the load. Figure 2g shows a 12-switch APF with a feedback harmonic detection scheme. This prototype is equipped with two PI controllers, which make the current harmonics feasible to detect. Finally, an eight-switch dual parallel full bridge inverter is proposed in Figure 2h, which is almost conventional to the current compensation concept. These topologies are the eight kinds of APFs introduced for the non-linear current compensation so far.

The proposed hybrid APF schematic is presented in Figure 3, containing both shunt passive and shunt active power filters with novel control system-based sliding mode control (SMC).
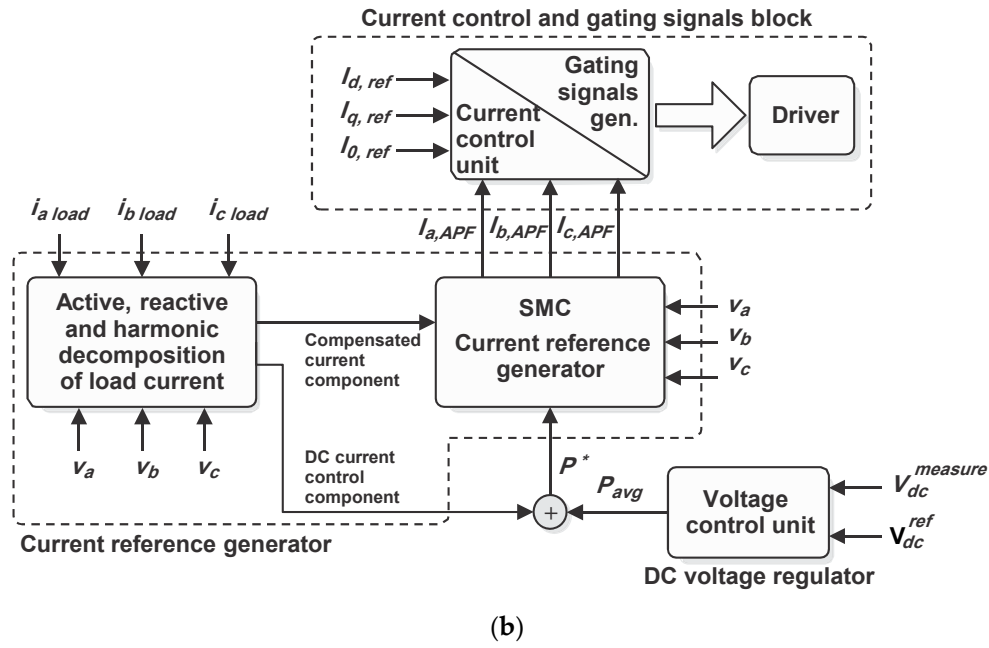

(**a**)

Figure 3. *Cont.*

(b)
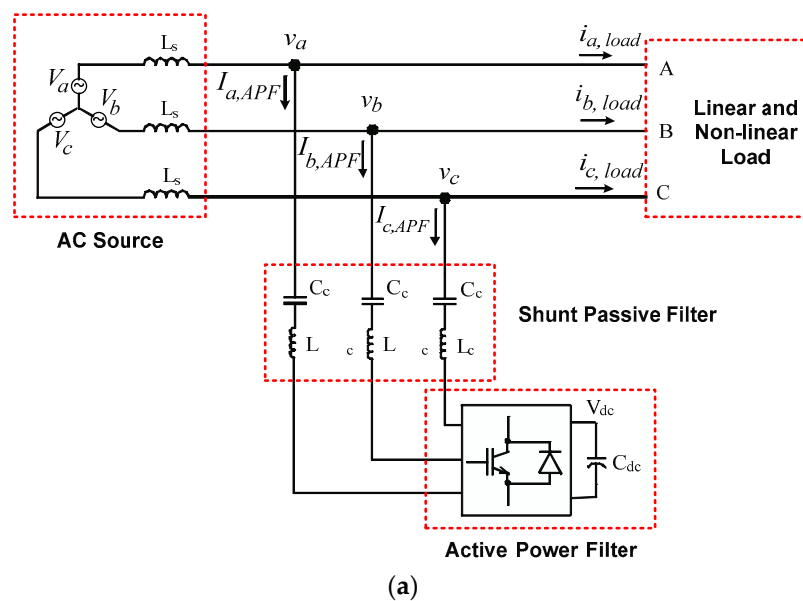
Figure 3. HAPF scheme; (**a**) Shunt APF with series in passive filter, (**b**) control diagram.

The state-space equations of the HAPF are mathematically formulated in Equation (1):

$$
\begin{aligned}
L_c \frac{d(i_{AFP,d})}{dt} &= \omega L_c i_{AFP,d} - v_{Cd} - u_d V_{dc} + v_{Ld} \\
L_c \frac{d(i_{AFP,q})}{dt} &= -\omega L_c i_{AFP,d} - v_{Cq} - u_q V_{dc} + v_{Lq} \\
C_c \frac{d(v_{cd})}{dt} &= i_{AFP,d} + \omega C_c v_{Cd} \\
C_c \frac{d(v_{cq})}{dt} &= i_{AFP,q} - \omega C_c v_{Cq}
\end{aligned}
\tag{1}
$$

where $i_{AFP,d}$ and $i_{AFP,d}$ are the *dq* frame compensating currents, the passive filter voltages in the *dq* frame are v_{Cd} and v_{Cq}, respectively, and v_L is the point of common coupling (PCC) voltage. The base equation for DC link capacitance is found in Equation (2).

$$
C_{dc} \frac{d(V_{dc})}{dt} = u_q i_{AFP,q} + u_d i_{AFP,d}
\tag{2}
$$

Therefore, the state-space equations of the above-mentioned relations in normal format are gathered in Equation (3).

$$
\begin{aligned}
\frac{d}{dt} X &= A(X) + B(X)u \\
Y &= C(X) + D(X)u
\end{aligned}
\tag{3}
$$

where the matrixes X, u, $A(X)$, $B(X)$, $C(X)$, and $D(X)$ are given as follows:

$$
\begin{aligned}
X &= \begin{bmatrix} i_{AFP,q} , & i_{AFP,d} , & v_{Cd} , & v_{Cq} \end{bmatrix}^T \\
u &= \begin{bmatrix} u_d , & u_q \end{bmatrix}^T
\end{aligned}
\tag{4}
$$

where the matrixes are represented in detail in Equation (5).

$$A(X) = \begin{bmatrix} \frac{1}{L_c}\left(\omega L_c i_{AFP,d} - v_{Cd} - u_d V_{dc} + v_{Ld}\right) \\ \frac{1}{L_c}\left(-\omega L_c i_{AFP,d} - v_{Cq} - u_q V_{dc} + v_{Lq}\right) \\ \frac{1}{C_c}\left(i_{AFP,d} + \omega C_c v_{Cd}\right) \\ \frac{1}{C_c}\left(i_{AFP,q} - \omega C_c v_{Cq}\right) \\ 0 \end{bmatrix}$$

$$B(X) = \begin{bmatrix} \frac{1}{L_c}(-V_{dc}) & 0 \\ 0 & \frac{1}{L_c}(-V_{dc}) \\ 0 & 0 \\ 0 & 0 \\ \frac{1}{C_c}(i_{cd}) & \frac{1}{C_c}(i_{cq}) \end{bmatrix} \tag{5}$$

$$C(X) = \begin{bmatrix} i_{AFP,d} \\ i_{AFP,q} \end{bmatrix}$$

$$D(X) = 0$$

Based on multi-input multi-output (MIMO) control system concepts, around the set point of load feeding, the linearization has been done using the Jacobean matrixes as below:

$$A_L = \begin{bmatrix} \frac{\partial A_1(X)}{\partial x_1} & \cdots & \frac{\partial A_1(X)}{\partial x_n} \\ \vdots & \ddots & \vdots \\ \frac{\partial A_n(X)}{\partial x_1} & \cdots & \frac{\partial A_n(X)}{\partial x_n} \end{bmatrix}$$

$$B_L = \begin{bmatrix} \frac{\partial B_1(X)}{\partial u_1} \\ \vdots \\ \frac{\partial B_n(X)}{\partial u_n} \end{bmatrix}. \tag{6}$$

Therefore, the linear system is defined as shown in Equation (7).

$$\frac{d}{dt}X = A_L X + B_L u + H + h \tag{7}$$

where h represents the outgoing/external limited attenuations, and H corresponds to the indeterminate matrix part of the linearized state space model. Then, selecting the desired reference vectors as X_d, the error function is found in Equation (8):

$$E = X - X_d. \tag{8}$$

Substituting Equation (8) for Equation (7) yields that:

$$\frac{d}{dt}E = A_L E + B_L u - \frac{d}{dt}X + \Delta H + \Delta h. \tag{9}$$

Utilizing high-order sliding mode control approaches will be useful to remove the chattering effect in switching functions. Thus, in order to delete the steady-state system error, the sliding surface is chosen as shown in Equation (10).

$$\vartheta = k_1 E + k_2 \int_0^t E\, dt \tag{10}$$

where k_1 and k_2 are constant vectors. Using the differentiate from Equation (10) will result in:

$$\frac{d}{dt}\vartheta = k_1\left(A_L E + B_L u - \frac{d}{dt}X + A_L X_d + \Delta H + \Delta h\right) + k_2 E. \tag{11}$$

The main idea for implementing SMC in this control system is described in the following. In the first step, the sliding surface (ϑ) is defined regarding the tracking error. In the second step, the inputs are designed due to ϑ being obtained. In the third step, ϑ and its derivative must turn in to get a zero amount. In other words, the system paths leading to the $\vartheta - \dot{\vartheta}$ plane are converged to the balance point with equation $\vartheta = \dot{\vartheta} = 0$. This definition is plotted in Figure 4.
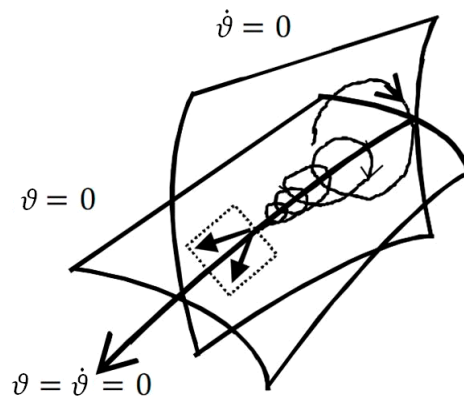

Figure 4. Convergence paths of the proposed controller.

Using the derivative from Equation (11) to achieve the second-order SMC is conducted to:

$$\frac{d^2}{dt^2}\vartheta = \left(k_1 A_L^2 + k_2 A_L\right) + k_1 A_L B_L u + \left(k_1 A_L^2 + k_2 A_L\right)E + X_d - k_2 \frac{d}{dt}X_d - k_1 \frac{d^2}{dt^2}X_d$$
$$+ (k_1 A_L + k_2)(\Delta H + \Delta h) + k_1 \frac{d}{dt}(\Delta H + \Delta h) + k_1 B_L \frac{d}{dt}u. \tag{12}$$

If the possibility for reaching zero for ϑ and its derivative in steady state by using the $\dot{u}$ signal is obtainable, then the real input of the system is going to be achieved considering the integral of the $\dot{u}$ signal. Therefore, the multi-state SMC sliding surface is defined as shown in Equation (13).

$$S = \gamma\vartheta + \frac{d}{dt}\vartheta \tag{13}$$

where γ is constant, and to calculate $\dot{S}$, it could be done that:

$$\dot{S} = \gamma\frac{d}{dt}\vartheta + \frac{d^2}{dt^2}\vartheta = \left(k_1 A_L^2 + k_2 A_L + \gamma k_1 A_L + \gamma k_2\right)E + (k_1 A_L B_L + k_2 B_L + \gamma k_1 B_L)u$$
$$+ \left(k_1 A_L^2 + k_2 A_L + \gamma k_1 A_L\right)X_d - (\gamma k_1 + k_2)\frac{d}{dt}X_d - \frac{d^2}{dt^2}X_d + k_1 B_L \frac{d}{dt}u$$
$$+ (\gamma k_1 A_L + \gamma k_2 + \gamma k_1)(\Delta H + \Delta h) + k_1 \frac{d}{dt}(\Delta H + \Delta h). \tag{14}$$

In the next step, the control law (u) should be used to justify the following equation.

$$S \times \frac{d}{dt}S < 0 \tag{15}$$

To obtain the rule explained in Equation (15) and converge exponentially, we should have:

$$\frac{d}{dt}S = -m_1 S - m_2 sign(S) \tag{16}$$

where m_1 and m_2 are positive constant coefficients. In this way, a suitable control rule should be defined for a closed loop system to place the state variable on a sliding surface. Using the Lyapunov function written in Equation (17) will guarantee the system's stability.

$$V = \frac{1}{2} S^2 \tag{17}$$

To ensure the stability of the whole system, the first derivative of the aforementioned Lyapunov function must by semi-definite negative. Therefore, we have:

$$\begin{aligned}
\frac{d}{dt}V = S \times \frac{d}{dt}S = S\Big\{&\big(k_1 A_L^2 + k_2 A_L + \gamma k_1 A_L + \gamma k_2\big)E + (k_1 A_L B_L + k_2 B_L + \gamma k_1 B_L)u \\
&+\big(k_1 A_L^2 + k_2 A_L + \gamma k_1 A_L\big)X_d - (\gamma k_1 + k_2)\frac{d}{dt}X_d - \frac{d^2}{dt^2}X_d + k_1 B_L \frac{d}{dt}u \\
&+(\gamma k_1 A_L + \gamma k_2 + \gamma k_1)(\Delta H + \Delta h) + k_1 \frac{d}{dt}(\Delta H + \Delta h)\Big\}
\end{aligned} \tag{18}$$

Substituting Equation (14) to Equation (16) results in:

$$\begin{aligned}
\dot{u} = -(k_1 B_L)^{-1}\Big\{&\big(k_1 A_L^2 + k_2 A_L + \gamma k_1 A_L + \gamma k_2\big)E + (k_1 A_L B_L + k_2 B_L + \gamma k_1 B_L)u \\
&+\big(k_1 A_L^2 + k_2 A_L + \gamma k_1 A_L\big)X_d + m_1 S + m_2 sign(S)
\end{aligned} \tag{19}$$

where the uncertainties and external attenuation applied to the reference vector are considered to be zero. The vector $(k_1 B_L)^{-1}$ is non-zero, which has been obtained by the proper designing of the sliding surface coefficient k_1. Substituting Equation (19) in Equation (18) results in:

$$\begin{aligned}
\frac{d}{dt}V = S\Big\{&-m_1 S - m_2 sign(S) + (\gamma k_1 A_L + \gamma k_2 + \gamma k_1)(\Delta H + \Delta h) + k_1 \frac{d}{dt}(\Delta H + \Delta h) \\
&-(\gamma k_1 + k_2)\frac{d}{dt}X_d - \frac{d^2}{dt^2}X_d\Big\} = -m_1 S^2 + m_2|S| + T.S.
\end{aligned} \tag{20}$$

To ensure that the equation investigated in Equation (20) is negative, we should have:

$$m_1 > 0 \tag{21}$$

$$\begin{aligned}
m_2 > &(\gamma k_1 A_L + \gamma k_2 + \gamma k_1)(\Delta H + \Delta h) + k_1 \frac{d}{dt}(\Delta H + \Delta h) - (\gamma k_1 + k_2)\frac{d}{dt}X_d \\
&-\frac{d^2}{dt^2}X_d - m_1 S = T.sign(S) - m_1|S|.
\end{aligned} \tag{22}$$

Finally, using integral operator applied to Equation (19) will obtain the control rule as below:

$$\begin{aligned}
u = -(k_1 B_L)^{-1} \int_0^t \Big\{&\big(k_1 A_L^2 + k_2 A_L + \gamma k_1 A_L + \gamma k_2\big)E + (k_1 A_L B_L + k_2 B_L + \\
&\gamma k_1 B_L)u + \big(k_1 A_L^2 + k_2 A_L + \gamma k_1 A_L\big)X_d + m_1 S + m_2 sign(S)\Big\} dt'
\end{aligned} \tag{23}$$

Since in some systems, there are no available approaches to obtain the upper limitation, the adaptive method is very useful in these conditions whether it is known or not. Therefore, the adaptive rule is hired to obtain the m_2 coefficient according to Equation (23). Thus, Equation (23) will be updated as shown in Equation (24).

$$\begin{aligned}
u = -(k_1 B_L)^{-1} \int_0^t \Big\{&\big(k_1 A_L^2 + k_2 A_L + \gamma k_1 A_L + \gamma k_2\big)E + (k_1 A_L B_L + k_2 B_L + \gamma k_1 B_L)u \\
&+\big(k_1 A_L^2 + k_2 A_L + \gamma k_1 A_L\big)X_d + m_1 S + \hat{m}_2 sign(S)\Big\} dt'
\end{aligned} \tag{24}$$

where $\hat{m}_2$ represents the uncertainties upper limitation. To adopt it with an adaptive rule, we should have:

$$\widetilde{m_2} = \hat{m}_2 - m_2 \tag{25}$$

where m_2 is the real gain and $\hat{m}_2$ represents the error estimation. According to [31], it can be mathematically stated with Equation (26).

$$\dot{\hat{m}}_2 = \frac{1}{\alpha}|S| \tag{26}$$

where α is a positive constant and $m_2(0)$ represents the initial condition. Since the sliding surface (S) at an infinite time of ϑ must reach zero, the adaptive estimation of error of $\hat{m}_2$ is limited. Therefore, to analyze the stability of the adaptive rule, a new Lyapunov function is defined as shown in Equation (27).

$$V = \frac{1}{2}S^2 + \frac{1}{2}\alpha\,\widetilde{m_2}^2 \tag{27}$$

Using the first-order derivative for Equation (27) results in:

$$\frac{d}{dt}V = S \times \frac{d}{dt}S + \alpha\,\hat{m}_2\,\dot{\hat{m}}_2 < S(T - m_1S - \hat{m}_2\,sign(S)) + \alpha(\hat{m}_2 - m_2) + \dot{\hat{m}}_2 \ < T.S - m_1S^2 - m_2|S| < 0. \tag{28}$$

The un-equality written in Equation (28) is valid for $m_2 > T.sign(S) - m_1|S|$ and then, since at an infinite time, the ϑ may not be completely zero, then the adaptive parameter $\hat{m}_2$ can increase as time goes on. Therefore, to solve this problem is to define the $\dot{\hat{m}}_2$ in the dead area as shown in Equation (29).

$$\dot{\hat{m}}_2 = \begin{cases} \frac{1}{\alpha}|S| & |S| > \varepsilon \\ 0 & |S| < \varepsilon \end{cases} \tag{29}$$

where ε is a real positive constant coefficient. By the way, the adaptive gain α is designed lower than the undefined system limitation to achieve the best results.

Thus, the injected current of the APF and the load voltage are ready to achieved as follows using Fourier transform in Equation (30).

$$\begin{aligned} I(t) = \ &\frac{A_{00}}{2} + \sum_{n=1}^{\infty}\left[A_{0n}\cos(n\omega_0 t) + B_{0n}\sin(n\omega_0 t)\right] \\ &+ \sum_{m=1}^{\infty}\left[A_{m0}\cos(m\omega_c t) + B_{m0}\sin(m\omega_c t)\right] \\ &+ \sum_{m=1}^{\infty}\sum_{n=-\infty,n\neq 0}^{\infty}\left[A_{mn}\cos(n\omega_0 t + m\omega_c t) + B_{mn}\sin(n\omega_0 t + m\omega_c t)\right] \end{aligned} \tag{30}$$

where ω_0 and ω_c correspond to the dc component and the frequent components, respectively. The detailed formulations are explained in Equations (31) to (33).

$$A_{m_{odd}0} = \sum_{k=1}^{\infty}\left[\frac{1}{2k-1}B_{2k-1}(2(2m-1)\pi M)(1 + 3\cos(k\pi)\sin((2k-1)\theta))\right] \tag{31}$$

$$A_{m_{odd}n_{even}} = \sum_{k=1}^{\infty}\left[B_{2k-1}(2(2m-1)\pi M)(P(n) + P(-n))\right]$$
$$P(n) = \frac{\cos(n\pi)\ + 3\cos(k\pi)\sin((2n+2k-1)\theta)}{2n+2k-1} \tag{32}$$

$$A_{m_{even}n_{odd}} = \sum_{k=1}^{\infty}\left[\cos(k\pi)B_{2k-1}(2(2m)\pi M)\left(\frac{\sin(2(n-k-1)\theta)}{n-k-1} + \frac{\sin(2(n+k)\theta)}{n+k}\right)\right] \tag{33}$$

where B_k represents the kth order of the Bessel function and M shows the modulation index.

Theorem 1 . *If the pur -sinusoidal load current is going to be obtained, therefore, an extra term exists in the q-axis component of the compensated current $I_{qq,comp}$, in which the model of the unwanted harmonics must be equal to zero. Thus, we have:*

$$I_{q,comp,APF} + I_{d,comp,APF} = \left(I_{q,DC,APF} + I_{qq,comp,APF} + \sum_{m=1}^{N} I_{q,load} \cos\left(m\omega t + \varphi_{q0}\right) \right)$$
$$+ \left(I_{d,DC,APF} + \sum_{m=1}^{N} I_{d,load,APF} \cos(m\omega t + \varphi_{d0}) \right). \tag{34}$$

In dynamic stability analysis, it is found that [29–31]:

$$I_{d,DC,APF} \geq \left(\frac{1}{2} \sum_{m=1}^{N} I_{q,load}^2 + I_{d,load}^2 \right)^{\frac{1}{2}} \tag{35}$$

$$I_{qq,comp,APF} = \left(I_{q,DC,APF}^2 - \frac{1}{2} \sum_{m=1}^{N} I_{q,load}^2 + I_{d,load}^2 \right)^{\frac{1}{2}} - I_{q,comp,APF}.$$

Due to the model definition described in Equation (5), the capacitor's low voltage is deduced in Equation (36).

$$\frac{dv_{cd}}{dt} = \frac{1}{C_c}\left(i_{AFP,d} + \omega C_c v_{Cd} \right)$$
$$\frac{dv_{cq}}{dt} = \frac{1}{C_c}\left(i_{AFP,q} - \omega C_c v_{Cd} \right) \tag{36}$$
$$\frac{dv_{C_{dc}}}{dt} = \frac{1}{C_{dc}}\left(i_{AFP,d} u_d + i_{AFP,q} u_q \right)$$

By substituting Equations (1) and (36) to (35) for all current harmonics, we have:

$$v_{cd} = \frac{1}{\omega C_c}\left(I_{q,DC,APF} + I_{qq,comp,APF} + \sum_{m=1}^{N} A_m \sin(m\omega t) + B_m \cos(m\omega t) \right)$$
$$v_{cq} = \frac{1}{\omega C_c}\left(-I_{q,DC,APF} + \sum_{m=1}^{N} C_m \sin(m\omega t) + D_m \cos(m\omega t) \right) \tag{37}$$

where A_m, B_m, C_m, and D_m can be calculated using Fourier transform. It is not simple to calculate the $I_{qq,comp}$ component directly, but if a new positive variable is defined as $\rho = v_{dc}^2$; therefore, by using an additional PI loop, the $I_{qq,comp}$ component will be maintained as below:

$$I_{qq,comp} = \left(k_p + \frac{k_i}{s} \right)(\rho - \rho^*) = k_p(\rho - \rho^*) + k_i \int_0^t (\rho - \rho^*) \, dt' \tag{38}$$

where v_{dc} represents the small signal component of the APF input voltage and $\rho^* = V_{dc}^2$ is the reference DC voltage.

3. Experimental Results

In order to verify and validate the effectiveness of the proposed converter and the control method, a laboratory setup is constructed and assembled (Figure 5) due to the specifications given in Table 1. In these laboratory tests, the converter is first tested under linear load and then with a non-linear load to check the performance of the provided active filter. The linear load is considered to be a balanced three-phase grounded resistive-inductive branch that makes the current flow drawn from all phases be equal. In the following, a non-linear load (diode rectifier and unequal resistive-inductive loads in each phase) is considered as the inverter output. Figure 6 shows the waveforms of the load voltage, load current, source current, and current injected by the filter. As it can be observed, the load voltage is completely sinusoidal, with an estimated total harmonic distortion (THD) as 1.3%.
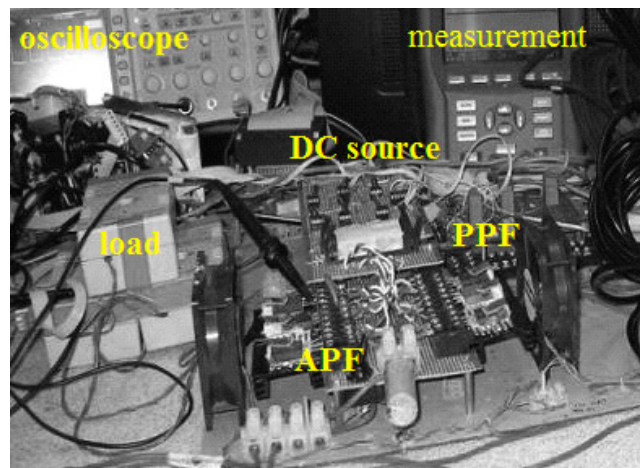
Figure 5. Proposed APF prototype used in laboratory tests.

Table 1. Prototype specifications. PPF: passive power filter.

| Parameter	Description	Value (SI)	Implemented Device
V_{AC}	AC grid voltage, Phase to ground	220 V, rms	AC power source
f_{line}	AC line/grid frequency	50 Hz	Function generator
f_{sw}	Switching frequency	12 kHz	Function generator
V_{DC}	DC link voltage	380 V	DC power supply
C_{DC}	DC link capacitance	4 mF	Constant type
L_C	PPF inductance	1.5 mH	Single coil
C_C	PPF capacitance	220 uF	Constant type
MOSFET	Power switches	600 V, . A	R6006KNX
D_{inv}	Power diodes	800 V, 2. A	VS-20ETS08
DSP	Programmer	Digital Signal Processor	TMS320C6748
$R - L$	Linear load	$60 \, \Omega + 0.1$ H	Constant type
$R - L - Rectifier$	Non-linear load	$60 \, \Omega + 0.1$ H	Rectifier: VS-T20HF220

(a)

(b)

(c)

(d)
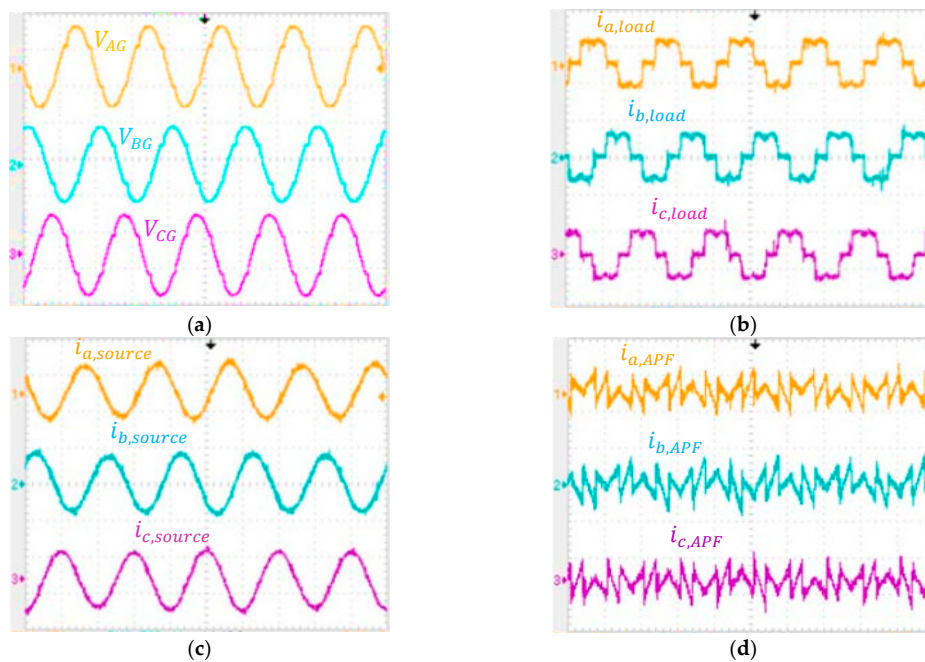
Figure 6. Experimental results at normal condition; (**a**) three-phase line-to-ground load voltages [volt/div: 220 V and time/div: 10 ms], (**b**) three-phase load currents [Amp/div: . A and time/div: 10 ms], (**c**) three-phase source currents [Amp/div: . A and time/div: 10 ms], (**d**) three-phase APF current injected to the load [Amp/div: . A and time/div: 10 ms].

The current injected by the APF is completely non-linear, making the current drawn from the source totally sinusoidal. In fact, the mathematical relation $I_{source} = I_{APF} + I_{load}$ causes the harmonic deficiencies of the load current to be compensated by the APF, so that the three-phase source does not endure high current stress and does not produce needle-shaped and pulsating currents. Figure 7 shows the THD coefficient for the source current and load current of phase *A*. As shown in this Fourier spectrum at Figure 7a, the source current THD is equal to 1.33% and always produces a sinusoidal current, because the rest of the non-linear load current is supplied by the APF, as shown in Figure 7b. The APF current THD at phase *A* is approximately 23.89%, indicating practically the complete compensation of load current harmonics. The source current fundamental harmonic is a little smaller than the load current, because the non-linear part of the load current is procured by the APF.
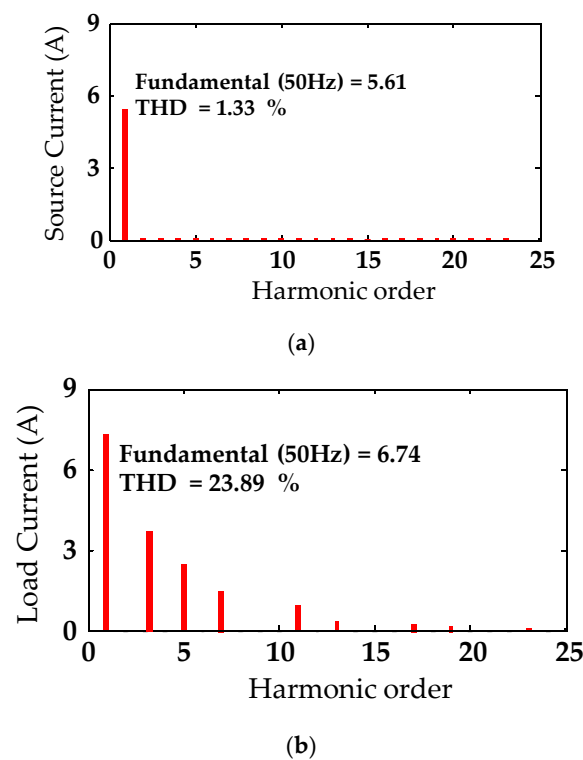

(**a**)

(**b**)

Figure 7. Current THD; (**a**) source current, (**b**) load current.

The experimental results for the three-phase average active and reactive power of the AC source in the base case (scenario 1) is presented in Figure 8. It is worth mentioning that this figure is obtained by multiplying the source voltage and current.
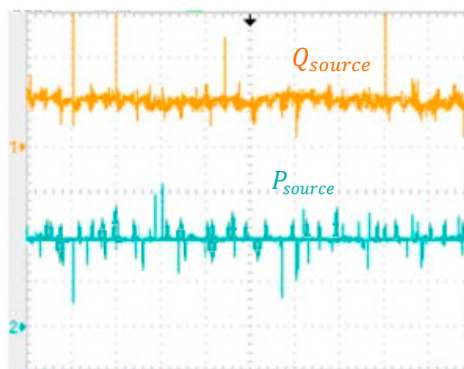

Figure 8. Experimental results for average reactive power compensation [VA/div: 1000 VA and time/div: 10 ms].

In the second scenario, the transient performance of APF is investigated. It is assumed that the hybrid APF is not connected to the grid initially. Formerly, the APF connects to the load in parallel to compensate for the non-linearity. Figure 9 represents the output waveforms of this experimental part. As it is observed, the load current is completely non-linear over the entire testing period, because the load has not been varied ever. The APF current is zero initially; however, after some time, it begins to compensate for the load current, resulting in the source current being pure sinusoidal (the purple graph). The green plot shows the DC link voltage, which is kept constant at all the experimented time intervals. These accurate results have predicated the effectiveness and applicability of the proposed control approach.
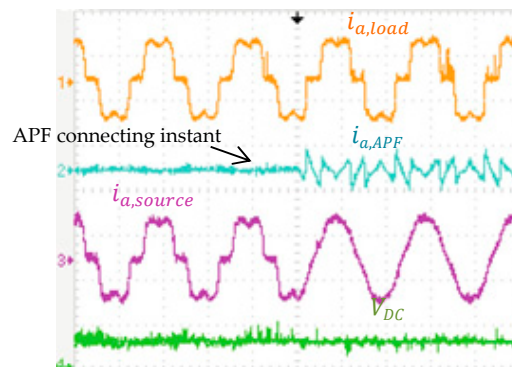
Figure 9. Experimental results at the transient condition; (**the orange color**) the load current wave form of phas. A [Amp/div: . A and time/div: 10 ms], (**the blue color**) the APF current wave form of phas. A [Amp/div: . A and time/div: 10 ms], (**the pink color**) the source current wave form of phas. A [Amp/div: . A and time/div: 10 ms], (**the green color**) the DC link voltage [volt/div: 500 V and time/div: 10 ms].

The third scenario describes the non-linear load increasing from a half load to full load. In this case, the load current driven at the 50% mode, which is half the total demand at the full load, as measured in the yellow color shown in Figure 10. However, the non-linear characteristic of the load has not been changed at all, and only its amplitude has grown up. The source current and APF current have also increased substantially to supply all the load demand. A DC link voltage diagram shows that at the moment of the load increasing, a voltage drop is observed. This voltage drop will be corrected by the DC link voltage regulator loop after a certain period of time, and the voltage will return back to the value before the load variation.
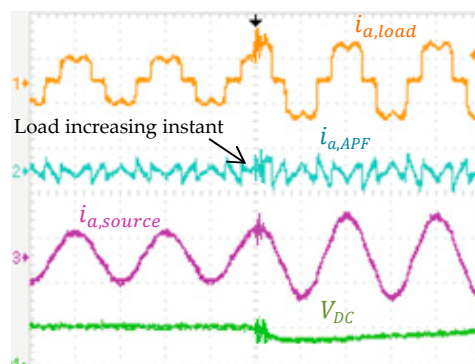
Figure 10. Experimental results at load variation condition; (**the orange color**) the load current wave form of phas. A [Amp/div: . A and time/div: 10 ms], (**the blue color**) the APF current wave form of phas. A [Amp/div: . A and time/div: 10 ms], (**the pink color**) the source current wave form of phas. A [Amp/div: . A and time/div: 10 ms], (**the green color**) the DC link voltage [volt/div: 500 V and time/div: 10 ms].

One of the important parameters that should be illustrated in the performance evaluation comparison of APFs is the THD in source current and load voltage. This is because the non-sinusoidal current source reduces the power source lifetime, indicating inappropriate filter performance. Figure 11 compares the THD of the source current with respect to the root mean square (*rms*) load voltage in different methods. It is noted that THD obtained from the proposed control strategy at all the voltage levels is lower than those of the existing methods, and this is proof of the proper controller performance. The comparison results shown in Figure 10 only have been conducted out in theory and simulation and the VSIs presented in [9] and [27] were not practically built in our laboratory. Their THD is calculated only in simulations and under load voltage variations in the same situations. The control methods used in [9] and [27] are "adaptive fuzzy neural network" and "Kalman filter integrated with wavelet transform", respectively. The first approach needs an extra module to adapt the membership function with a neural network, resulting in much data analysis volume and a lower response computation speed. The second one uses Kalman filter to estimate the unknown vectors of the load current FFT spectrum, and discrete wavelet transform (DWT) is used for harmonic detection. However, the proposed control approach only needs some constant SMC coefficients to insure the Lyapunov function stability with high-speed convergence. According to these explanations, much of the data analysis causes the load current not to be compensated completely, and as a result, the SMC approach is more suitable to control the APF at non-linear conditions compared with those other strategies.
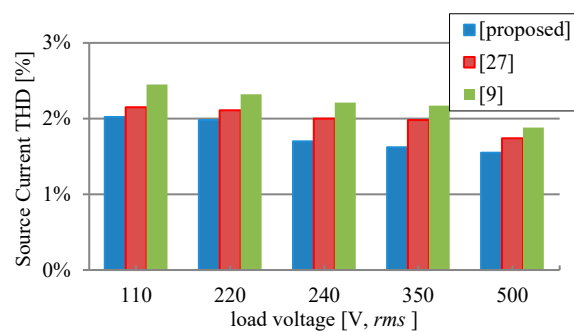
Figure 11. Source current THD in terms of load voltage.

A number of control theories of HAPFs such as instantaneous reactive power theory, synchronously rotating frame theory, and many more with several low-pass, high-pass, and band-pass digital filters along with several closed-loop controllers such as the proportional–integral (PI) controller, the adaptive fuzzy neural network (AFNN), etc., have been employed to implement HAPFs. Moreover, many manufacturers are developing HAPFs even at quite large power ratings to improve the power quality of a vast range of non-linear loads [30]. However, in this way, the most appropriate and easy to implement control approach are the main factors. The significant reasons why we use SMC are listed below in bullet and numbers:

1. The SMC coefficients are easy to regulate based on the Lyapunov function and its first-order derivative, while the other approaches have some disadvantages such as:

   ○ Proportional–integrator (PI): cannot be used in wide range of operation, and it is not able to eliminate the dynamic errors perfectly.
   ○ Fuzzy neural network (FNN) or adaptive FNN: uses large training data volume to calculate the rules and implement the membership functions, the numbers of rules may be increased, there are errors in the de-fuzzier block, and it uses high processing time for large systems.
   ○ Kalman filter integrated with wavelet transform: error in estimations and detections, error in uncorrelated and correlated data selection, error in calculation DWT coefficients.

    ○   Genetic algorithm (GA)-based PI: hard to find the global optimum, certain optimization problems cannot be solved due to poorly known fitness functions, which generate bad chromosomes.

    ○   Particle swarm optimization (PSO)-based PI: sometimes, the PSO algorithm fails to find the required optimas when the problem to be solved is highly complicated.

    ○   Bacteria foraging optimization (BFO)-based PI: although the convergence speed is faster than GA and PSO, the drawback of the BFO algorithm is its fixed step size, which reduces its average rate.

2. The SMC convergence used in this work is exponentially obtainable, resulting in a high-speed response for load current tracking.
3. No extra complicated transform or membership function or neural network is needed to run the simulation.
4. Proper sliding surface selection has a powerful capability for signal tracking.
5. Good dynamic response can be achieved by SMC as proved in many studies in the literature.

The only current research gap is that the load current is not completely compensated with a precise sinusoidal-shaped waveform. Although the presented strategy achieves better results than the others mentioned above, still, the complete harmonic current compensation ($THD_{I_{Source}} = 0$) is a major research topic for those scholars interested in APF.

The experimental and theoretical verifications of system efficiency are also added to the manuscript due to the output *rms* load current variation, as shown in Figure 12. This verification implies that the proposed prototype is working successfully with high efficiency and reliable performance.
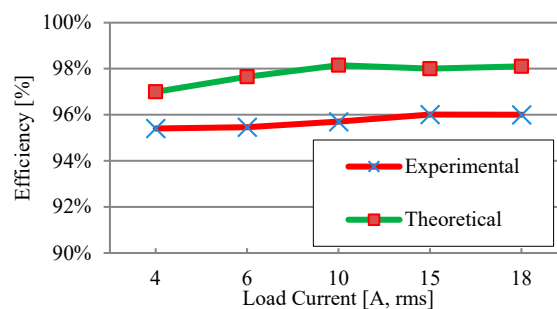

Figure 12. Experimental and theoretical efficiency analysis.

4. Conclusions

In this paper, an improved hybrid APF combined with a series PPF is introduced that compensates the required harmonic load current using the SMC control method. Under the proposed control method, three scenarios were implemented in the laboratory, summarizing the results as follows:

- The non-linear loads existing in power networks can easily be compensated without losing network stability. This is proved by using the Lyapunov function and selecting the appropriate controller coefficients.
- The transient behavior of the load variation in the power system may lead to large-scale instability and perturbations in the absence of suitable control methods. The proposed approach can prevent such occurrences by using only one hybrid APF.
- The proposed APF responds quickly to non-linear loads and compensates for the non-linear currents without any delay. This issue has been described in the second scenario.
- An additional voltage control loop for DC link voltage can minimize the fluctuations and prevent disturbance to the AC output voltage amplitude.
- The load current magnitude has no effect on the APF performance provided, as fully tested in the third scenario.

- The reactive power compensation in the proposed APF causes the DC link voltage to return back to its initial range immediately after the contingency occurrence instant.

References

1. Fei, J.; Wang, H.; Cao, D. Adaptive back-stepping fractional fuzzy sliding mode control of active power filter. *Appl. Sci.* **2019**, *9*, 3383. [CrossRef]
2. Garces-Gomez, Y.A.; Hoyos, F.E.; Candelo-Becerra, J.E. Classic Discrete Control Technique and 3D-SVPWM Applied to a Dual Unified Power Quality Conditioner. *Appl. Sci.* **2019**, *9*, 5087. [CrossRef]
3. Hoon, Y.; Radzi, M.; Amran, M.; Al-Ogaili, A.S. Adaptive Linear Neural Network Approach for Three-Phase Four-Wire Active Power Filtering under Non-Ideal Grid and Unbalanced Load Scenarios. *Appl. Sci.* **2019**, *9*, 5304. [CrossRef]
4. Mahmoudian, M.; Gitizadeh, M.; Rajaei, A.H.; Tehrani, V.M. Common mode voltage suppression in three-phase voltage source inverters with dynamic load. *IET Power Electron.* **2019**, *12*, 3141–3148. [CrossRef]
5. Blasco, P.A.; Montoya-Mira, R.; Diez, J.M.; Montoya, R.; Reig, M.J. Compensation of Reactive Power and Unbalanced Power in Three-Phase Three-Wire Systems Connected to an Infinite Power Network. *Appl. Sci.* **2020**, *10*, 113. [CrossRef]
6. Molina, E.; Candelo-Becerra, J.E.; Hoyos, F.E. Control Strategy to Regulate Voltage and Share Reactive Power Using Variable Virtual Impedance for a Microgrid. *Appl. Sci.* **2019**, *9*, 4876. [CrossRef]
7. Song, S.; Hwang, S.; Ko, B.; Cha, S.; Jang, G. Novel Transient Power Control Schemes for BTB VSCs to Improve Angle Stability. *Appl. Sci.* **2018**, *8*, 1350. [CrossRef]
8. Blecharz, K.; Morawiec, M. Non-linear Control of a Doubly Fed Generator Supplied by a Current Source Inverter. *Energies* **2019**, *12*, 2235. [CrossRef]
9. Fei, J.; Wang, T. Adaptive fuzzy-neural-network based on RBFNN control for active power filter. *Int. J. Mach. Learn. Cybern.* **2019**, *10*, 1139–1150. [CrossRef]
10. Mahaboob, S.; Ajithan, S.K.; Jayaraman, S. Optimal design of shunt active power filter for power quality enhancement using predator-prey based firefly optimization. *Swarm Evol. Comput.* **2019**, *44*, 522–533. [CrossRef]
11. Yunus, H.I.; Bass, R.M. Comparison of VSI and CSI topologies for single-phase active power filters. *Inpesc Rec. 27th Annu. Ieee Power Electron. Spec. Conf.* **1996**, *2*, 1892–1898.
12. Pawar, R.; Gawande, S.; Nagpure, R.; Waghmare, M. Modified ISCA Based Control for Operating Electric Spring in Active Power Filter Mode. *IET Power Electron.* **2019**, *1*, 1.
13. Tang, Y.; Loh, P.C.; Wang, P.; Choo, F.H.; Gao, F.; Blaabjerg, F. Generalized design of high performance shunt active power filter with output LCL filter. *IEEE Trans. Ind. Electron.* **2011**, *59*, 1443–1452. [CrossRef]
14. Jauhari, M.; Riawan, D.C.; Ashari, M. Control Design for Shunt Active Power Filter Based On pq Theory in Photovoltaic Grid-Connected System. *Int. J. Power Electron. Drive Syst.* **2018**, *9*, 1064.
15. Narasimhulu, V.; Kumar, D.A.; Babu, C.S. Computational intelligence based control of cascaded H-bridge multilevel inverter for shunt active power filter application. *J. Ambient Intell. Humaniz. Comput.* **2020**, *4*, 1–9. [CrossRef]
16. Charalambous, A.; Hadjidemetriou, L.; Zacharia, L.; Bintoudi, A.D.; Tsolakis, A.C.; Tzovaras, D.; Kyriakides, E. Phase Balancing and Reactive Power Support Services for Microgrids. *Appl. Sci.* **2019**, *9*, 5067. [CrossRef]
17. Munir, H.; Zou, J.; Xie, C.; Guerrero, J. Cooperation of voltage controlled active power filter with grid-connected DGs in microgrid. *Sustainability* **2019**, *11*, 154. [CrossRef]
18. Kumar, R.; Bansal, H.O. Hardware in the loop implementation of wavelet based strategy in shunt active power filter to mitigate power quality issues. *Electr. Power Syst. Res.* **2019**, *1*, 92–104. [CrossRef]
19. Hou, S.; Fei, J.; Chen, C.; Chu, Y. Finite-time adaptive fuzzy-neural-network control of active power filter. *Ieee Trans. Power Electron.* **2019**, *34*, 10298–10313. [CrossRef]

20. Fujita, H.; Akagi, H. A practical approach to harmonic compensation in power systems-series connection of passive and active filters. *IEEE Trans. Ind. Appl.* **1991**, *27*, 1020–1025. [CrossRef]

21. Peng, F.Z.; Akagi, H.; Nabae, A. A new approach to harmonic compensation in power systems-a combined system of shunt passive and series active filters. *IEEE Trans. Ind. Appl.* **1990**, *26*, 983–990. [CrossRef]

22. Li, D.; Yang, K.; Zhu, Z.Q.; Qin, Y. A novel series power quality controller with reduced passive power filter. *IEEE Trans. Ind. Electron.* **2016**, *64*, 773–784. [CrossRef]

23. Biswas, P.P.; Suganthan, P.N.; Amaratunga, G.A. Minimizing harmonic distortion in power system with optimal design of hybrid active power filter using differential evolution. *Appl. Soft Comput.* **2017**, *61*, 486–496. [CrossRef]

24. Narongrit, T.; Areerak, K. Adaptive fuzzy control for shunt active power filters. *Electr. Power Compon. Syst* **2016**, *44*, 646–657. [CrossRef]

25. Wang, L.; Lam, C.S.; Wong, M.C. Selective compensation of distortion, unbalanced and reactive power of a thyristor-controlled LC-coupling hybrid active power filter (TCLC-HAPF). *IEEE Trans. Power Electron.* **2017**, *32*, 9065–9077. [CrossRef]

26. Luo, Z.; Su, M.; Sun, Y.; Zhang, W.; Lin, Z. Analysis and control of a reduced switch hybrid active power filter. *Iet Power Electron.* **2016**, *9*, 1416–1425. [CrossRef]

27. Swain, S.D.; Ray, P.K.; Mohanty, K.B. Design of Passive Power Filter for Hybrid Series Active Power Filter using Estimation, Detection and Classification Method. *Int. J. Emerg. Electr. Power Syst.* **2016**, *17*, 363–375. [CrossRef]

28. Tareen, W.U.; Mekhilef, S.; Seyedmahmoudian, M.; Horan, B. Active power filter (APF) for mitigation of power quality issues in grid integration of wind and photovoltaic energy conversion system. *Renew. Sustain. Energy Rev.* **2017**, *70*, 635–655. [CrossRef]

29. Mahmoudian, M.; Gitizadeh, M.; Bina, M.A. High Accuracy Power Sharing in Parallel Inverters in an Islanded Microgrid Using Modified Sliding Mode Control Approach. *Sci. Iran.* **2019**. In press. [CrossRef]

30. Singh, B.; Verma, V.; Chandra, A.; Al-Haddad, K. Hybrid filters for power quality improvement. *IEE Proc. -Gener. Transm. Distrib.* **2005**, *152*, 365–378. [CrossRef]

31. Jiang, B.; Karimi, H.R.; Kao, Y.; Gao, C. Reduced-order adaptive sliding mode control for nonlinear switching semi-Markovian jump delayed systems. *Inf. Sci.* **2019**, *477*, 334–348. [CrossRef]